Including gap region field-aligned currents and magnetospheric currents in the MHD calculation of ground-based magnetic field perturbations

Yiqun Yu,[1] Aaron J. Ridley,[1] Dan T. Welling,[1,2] and Gabor Tóth[1]

[1] Many high-latitude modeling studies utilize the horizontal ionospheric Hall current in calculating ground-based magnetic perturbations, but low-latitude and midlatitude studies should include current systems such as the magnetospheric, field-aligned, and Pedersen currents. Recently, by including all these current systems, a more precise ground-based perturbation calculator has been implemented in the Space Weather Modeling Framework. Using this new method, ground-based perturbations generated by different current systems are analyzed at low, middle, and high latitudes. As a result of the current systems, MLT-UT maps of ground-based perturbations are studied. Furthermore, nine storms events are simulated at more than 20 low-latitude and midlatitude magnetometer locations and compared with observational ground-based perturbations. These studies show that for specifying the northward component of the ground magnetic perturbations, the inclusion of magnetospheric, field-aligned, and Pedersen current is important and improves the prediction significantly over the prediction only considering the Hall current in the calculation. The improvement is the most during the storm main phase. However, for the vertical and eastward components of the perturbations, which were typically smaller than the northward component, the inclusion of these current systems actually made the specifications worse because the ring current in the model rotates more toward the dayside than in reality.

Citation: Yu, Y., A. J. Ridley, D. T. Welling, and G. Tóth (2010), Including gap region field-aligned currents and magnetospheric currents in the MHD calculation of ground-based magnetic field perturbations, *J. Geophys. Res.*, *115*, A08207, doi:10.1029/2009JA014869.

1. Introduction

[2] Most magnetohydrodynamics (MHD) modeling studies have made simplifications in calculating the ground magnetic perturbations that are induced by current systems around the Earth [*Raeder et al.*, 2001; *Shao et al.*, 2002; *Ridley et al.*, 2001; *Wiltberger et al.*, 2003; *Yu and Ridley*, 2008]. One common simplification is that these studies neglect the field-aligned current (FAC) and ionospheric Pedersen current in calculating the perturbations. This simplification is based on Fukushima's theorem, which states that the perturbation caused by FACs is canceled out by the Pedersen current under the conditions of uniform conductance and field lines perpendicular to the surface [*Fukushima*, 1976]. Another simplification is that these studies did not take into account the magnetospheric currents (including tail current, magnetopause current, ring current, and so on), assuming that these currents are far away from the ground. Therefore after these two assumptions, only the ionospheric Hall current is left to account for the ground-based perturbations.

[3] However, the two typical simplifications are imprecise for two reasons: (1) magnetic field lines are not vertical even in the auroral zone, let alone at midlatitudes, nor is the ionospheric conductivity uniform; rather, the conductivity is highly controlled by the solar EUV flux and auroral precipitation; and (2) at low and middle latitudes, the magnetospheric currents play an important role in controlling the intensity of magnetic perturbations. This control is especially true during storm times, when the ring current, which is represented by the D_{st} index, a proxy of energy level in the ring current, obtained by averaging ground perturbations from four low-latitude magnetometers, forms and strengthens. Therefore FACs, Pedersen currents, and magnetospheric currents should be included in any calculation of the ground magnetic perturbations, which could lead to more precise results. There was actually one attempt earlier by *Pulkkinen et al.* [2007a], who computed the ground magnetic perturbation at high latitudes by using the FACs, Hall, and Pedersen currents. But no magnetospheric currents were considered, since the authors were studying the high-latitude regions.

[4] While obtaining the current information in a global magnetosphere model and ionospheric electrodynamics

---

[1]Center for Space Environment Modeling, University of Michigan, Ann Arbor, Michigan, USA.
[2]Now at Los Alamos National Laboratory, Los Alamos, New Mexico, USA

model is easy, since both models solve current in all the grid points in their simulation domains, a numerical "gap" region exists between the ionosphere model and the inner boundary (usually at 2.5 to 3.5 R_e) of the global magnetosphere model. This "gap" region is numerically difficult to solve in the MHD code, first because the large magnetic field in this region, and thus high Alfvén wave speeds, requires the numerical time step to be extremely small in order to guarantee the stability of the code, and second because much higher resolution is needed to model the converging field lines near the Earth. These requirements of small time steps and high resolution are computationally expensive; therefore a "gap" region is utilized.

[5] This paper presents work on the inclusion of all the magnetospherically driven current systems within geospace (i.e., the Hall and Pedersen current in the ionosphere, FACs in the "gap" region, and the magnetospheric current, including both field-aligned and perpendicular current, since the MHD code handles both) to compute the ground-based magnetic field perturbations. Note that no criterion has yet been found to distinguish the various current systems in the magnetosphere model, such as ring current, tail current, magnetopause current, FAC, and so on; therefore these current systems are not separated but are referred to as magnetospheric current.

2. Technique

[6] This section describes the techniques used to extract the currents that, through the Biot-Savart law (equation (1)), induce the ground magnetic field perturbations

$$\Delta \vec{B}(\vec{r}) = \frac{\mu}{4\pi} \int \frac{\vec{J}' \times (\vec{r} - \vec{r}')}{|\vec{r} - \vec{r}'|^3} d\vec{r}'3 \qquad (1)$$

where $\vec{J}'$ is the current source, $\vec{r}'$ represents the position of the current source, $\vec{r}$ is the location of the magnetometer, and μ is the magnetic permeability of free space.

[7] The current systems from the ionosphere, the magnetosphere, and the "gap" region are adopted as the current sources for the perturbation calculation and are obtained by different methods. First, for the ionospheric current, *Powell et al.* [1999] and *Ridley et al.* [2001, 2002] incorporated the technique of solving the inner boundary conditions in the global MHD code Block-Adaptive Tree Solar wind Roe Upwind Scheme (BATSRUS). The boundary conditions drive an ionospheric electrodynamic model, from which ionospheric Hall and Pedersen currents are achieved with conductance patterns at the ionosphere [*Ridley et al.*, 2004]. Note that this high-latitude ionospheric electrodynamics model does not solve the solar daily variation Sq current and equatorial electrojet, which are low-latitude current systems. The ionospheric model here is simply height-integrated conductance in which the FACs from the magnetosphere are closed. Therefore the in situ generated ionosphere and thermosphere current systems (driven by the neutral winds) are not considered in our simulation calculation. Second, for the magnetospheric current, the global magnetospheric MHD model BATSRUS coupled with an inner magnetospheric model (the Rice Convection Model [*Wolf et al.*, 1982]) computes the current at each grid through the inductive equation $\vec{J} = \frac{1}{\mu} (\nabla \times \vec{B})$, in parallel while solving

the ideal MHD equations. Third, for the FACs in the "gap" region, a mapping technique is used along the presumed dipolar magnetic field lines. The mapping starts from a uniform grid boundary at 3 R_e shell, with a resolution of 1° in the latitude and 2° in the longitude. The FACs at any point along the field lines in this "gap" region then can be extracted by

$$\frac{J_{\|m}}{B_m} = \frac{J_{\|r}}{B_r} \qquad (2)$$

where $J_{\|m}$ and B_m are the FAC and the magnetic field at 3 R_e computed in the global magnetosphere model BATSRUS, and where $J_{\|r}$ and B_r represent the FAC and magnetic field at any position in the "gap" region. This mapping technique assumes no sources of field-aligned current in the "gap" region and no mirror current in the Earth that would amplify the perturbations measured by the ground-based magnetometers [*Pulkkinen et al.*, 2007b]. After obtaining these three current systems within the geospace system, the main focus of this study is the inclusion of more distant current systems, so the low-latitude and midlatitude magnetometer perturbations will be more accurately computed. In summary, the modeled ground-based perturbations are the sum of the perturbations caused by the ionospheric Hall and Pedersen currents at high latitude above 50°, the "gap" region FACs, and the magnetospheric currents.

3. Model-Data Comparison: One Example

[8] After taking all the current systems into account in calculating the perturbations in the MHD model, the simulation results are compared with the ground-based magnetometer observations at three individual stations. Comparisons are also carried out in two-dimensional maps in the magnetic local time-universal time coordinates. To quantify the agreement between the simulation predictions and the observations, the root-mean-square (RMS) error is utilized and then normalized by the RMS variation of the observations:

$$nRMS = \frac{\sqrt{\langle (\Delta B_p - \Delta B_o)^2 \rangle}}{\sqrt{\langle \Delta B_o^2 \rangle}}, \qquad (3)$$

where nRMS is the normalized root mean square error and ΔB is the magnetic field perturbation from the observation (ΔB_o) or the prediction (ΔB_p). The average is taken over the simulation time period. A nRMS error below 1 indicates that the simulation produces good agreement with the data, while a nRMS error above 1 indicates that the simulation misses the data significantly. A nRMS error equal to zero means the simulation produces exactly the same result as the data. It should be noted that while the simulated perturbations, as mentioned above, are not affected by the Sq current system or the equatorial electrojet, the observation data may be influenced by the equatorial electroject from the equator and the Sq current system, although the approximated effect of the Sq current has been removed by subtracting the median of the quiet time variations over 1 month.

3.1. Different Latitudes

[9] The geomagnetic storm event on 4 May 1998 is chosen for the data-model comparison. At 0315 UT, the
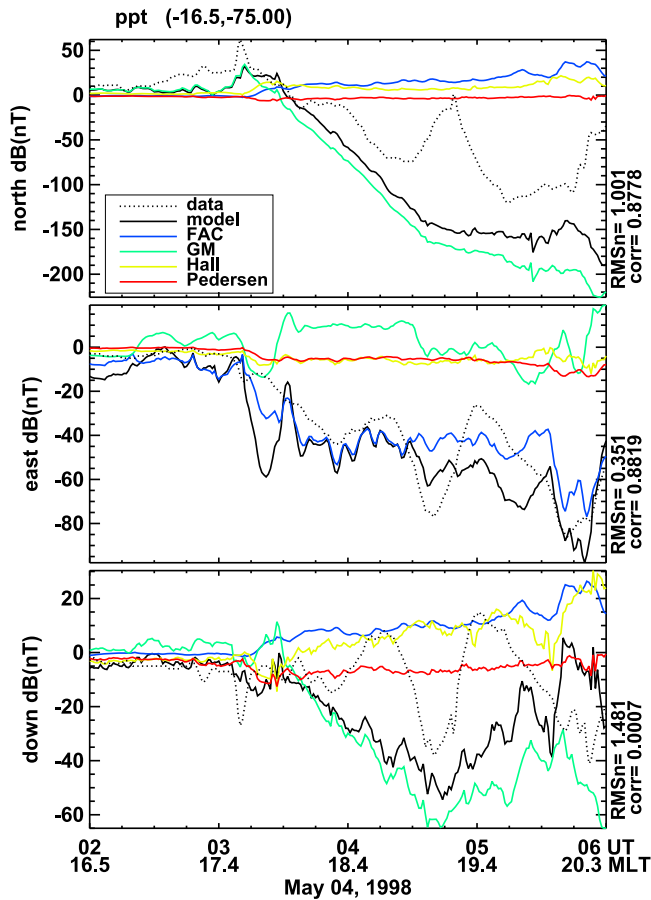
Figure 1. Three components of the ground magnetic perturbations at a low-latitude magnetometer PPT on 4 May 1998. The magnetic coordinate for the magnetometer is shown on the top. Black dashed line is observational perturbations. Solid lines are simulated perturbations; solid black is the total of the four individual current systems represented in different colors. The normalized RMS error and the cross-correlation coefficient between the simulated total perturbation and the observational perturbation are labeled on the right. On the bottom labels the universal time and the magnetic local time of this magnetometer.

solar wind and interplanetary magnetic field (IMF) become quite strong, with the solar wind density increasing up to 20/cc and with the southward IMF Bz increasing up to 30 nT. Figures 1, 2, and 3 illustrate the observational ground-based magnetic perturbations (black dashed lines), the simulated perturbations caused by individual current systems (color lines), and the simulated total perturbations from all these current systems (black solid lines) at three magnetometers. On the right side of Figures 1, 2, and 3 are labels for the nRMS errors and the cross correlation coefficients. On the bottom of Figures 1, 2, and 3 are shown the universal time and the magnetic local time for the corresponding magnetometers.

[10] Figure 1 shows three components of the magnetic perturbations at a low-latitude magnetometer PPT, which was located at around 16° south magnetic latitude on the duskside during the simulation time. Comparisons between the observed and the simulated total perturbations show

different features in the three components. In the northward component (Figure 1, top), the simulated perturbation roughly follows the trend of the observation with a high cross correlation coefficient of 0.87. However, the simulation misses the variation around 0445 UT in the data, leading to a large nRMS error of 1.001. In the eastward component (Figure 1, middle), the simulated total perturbation agrees relatively well with the observation with a small nRMS error of 0.351 and a high cross correlation coefficient of 0.88. In the downward component (Figure 1, bottom), the simulation perturbation misses the dynamical perturbations in the data, causing a large nRMS error and a tiny cross correlation coefficient. The two simulation-missed field enhancements observed in the data (dash line) at times 0415 and 0500 UT may result from the expansion of the equatorial electrojet from the dayside. The electrojet, flowing in the eastward direction near the equator, enhances during the storm and results in downward magnetic perturbations in the Southern Hemisphere [*Kobea et al.*, 1998]; however, the simulation does not consider this electrojet as mentioned earlier.

[11] In addition, the analysis of individual current-induced perturbations also indicates different features in the three components. In the northward component, the magnetospheric current (GM) dominates in obtaining the total per-
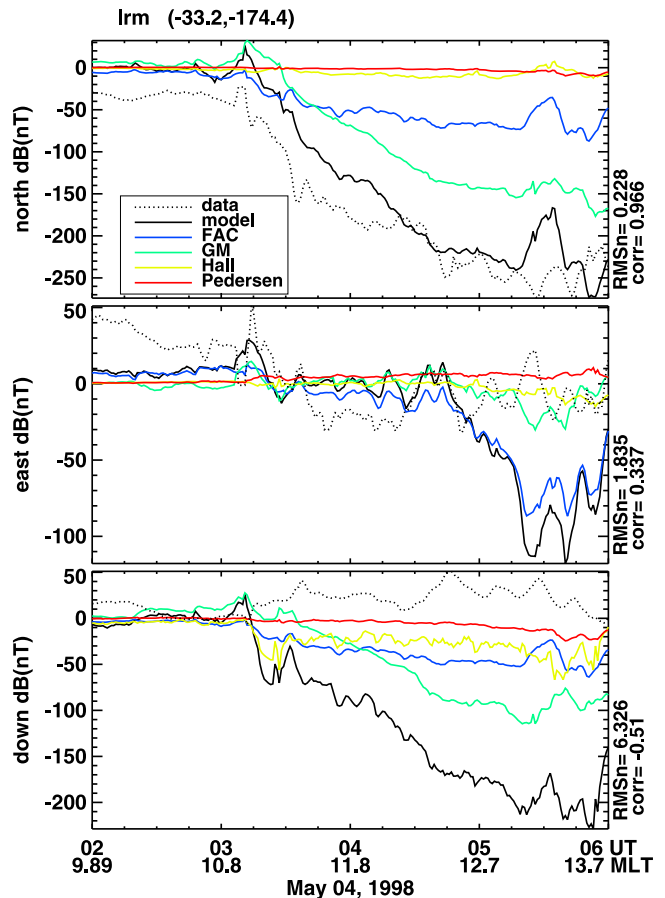

Figure 2. Three components of the ground magnetic perturbations at a midlatitude magnetometer LRM on 4 May 1998. They are in the same format as in Figure 1.
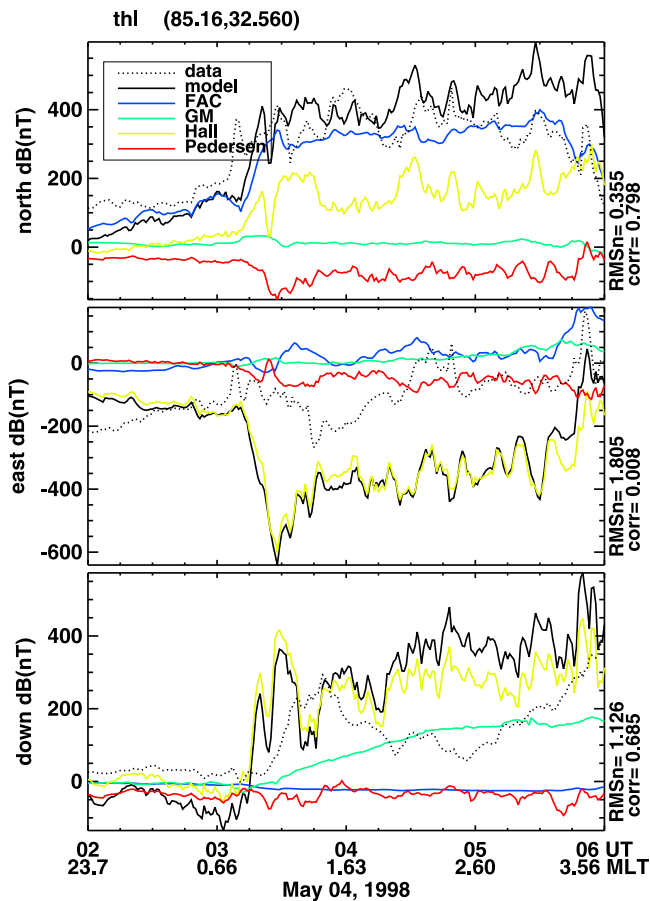
Figure 3. Three components of the ground magnetic perturbations at a high-latitude magnetometer THL on 4 May 1998. They are in the same format as in Figure 1.

turbations, while the ionospheric Pedersen current produces negligible perturbations, and the FACs and Hall current slightly contribute 10–30 nT. In the east component, the FACs, enhanced on the duskside during the storm time, mainly follow the simulated total perturbations, while the ionospheric current (Hall and Pedersen) make little contribution. In the downward component, the magnetospheric current (GM) results in upward perturbations and mainly follow the total simulated perturbations, and the Hall current and FACs also induce medium perturbations but in the opposite direction. Again, the Pedersen current results in negligible perturbations.

[12] Figure 2 shows the perturbations at a midlatitude magnetometer LRM, which was located at around 33° south magnetic latitude on the dayside. Comparisons between the observation and simulated total perturbations show that the model works well for the northward component but not in the other two components. In the northward component, the model roughly captures the trend and the magnitude of the observational perturbations, resulting in a high cross correlation coefficient of 0.966 and a small nRMS error of 0.228. In the eastward component, the modeled perturbations are largely westward after 0500 UT, but the data show roughly small westward perturbations. In the downward component,

the simulation misses the observation not only in the direction but also in the magnitude. In the last two components, the comparison shows large nRMS errors. This large discrepancy in the downward component could be caused by the improperly simulated FACs during this storm (discussed in the next section).

[13] Examination of individual current systems reveals that different current systems dominate over the others in different components. In the northward component, the magnetospheric current and FACs produce most of the perturbations at the midlatitude magnetometer, while the ionospheric current (Hall and Pedersen) can be neglected. In the eastward component, the FACs are the dominant generator of the total perturbations. The magnetospheric currents start to contribute some amount (a maximum of about 1/3) of the total perturbations after 0500 UT and the ionospheric currents (Hall and Pedersen) again can be neglected. In the downward component, all current systems seem to have contributions to the total perturbations but with different intensity. The magnetospheric current clearly plays the largest role in generating the total upward perturbations during the storm time. This large upward perturbation is actually caused by the westward ring current (detailed discussion will be in section 3.2). The Hall current and the FACs induce around 20–50 nT perturbations in the storm, while the Pedersen current produces 10–20 nT after 0530 UT.

[14] Figure 3 shows the perturbations at a high-latitude magnetometer THL, which was located at 85° north magnetic latitude on the dawnside. In the northward component, the modeled perturbations not only show similar trends to the observations but also comparable magnitudes, with a nRMS error of 0.35 and a cross correlation coefficient of 0.80. The FACs produce large perturbations, half of which, however, are nearly canceled by the perturbations from Pedersen current. The Hall current contributes roughly 50% of the total perturbations, while the magnetospheric current shows negligible perturbations. In the eastward component, the simulation generally follows the trends of the data but largely misses the magnitude. In this component, the perturbations caused by the Hall current dominates over the perturbations caused by any other current systems, while the perturbations caused by the FACs and Pedersen current partly cancel each other but not completely. The magnetospheric current again has little contribution. In the downward component the simulated result only partially follows the observational trends and magnitude. The Hall current again is the major generator of the total simulated perturbations, while the FACs, unlike in the other two components, show little contribution. The magnetospheric current, however, shows perturbations up to 150 nT during the storm time. These large perturbations are probably caused by the magnetopause current in the cusp region, as this magnetometer was very close to the North Pole. The analysis of the three components at high latitude validates that the Hall current is the dominant current system at high latitudes, but this current system cannot simply be adopted as the only current source for the perturbation calculation because the FACs and Pedersen current do not cancel each other completely (this was also found by *Chen et al.* [1982]), and the magnetospheric current might flow closely to the polar region.

3.2. Magnetic Local Time Dependence (MLT-UT Maps)

[15] In the previous section, individual current systems have been analyzed and ground-based magnetic perturbations from the simulation and the data at three magnetometers from low, middle, and high latitudes, respectively, have been compared. The comparison shows that the model can predict the magnetic perturbations at low and middle latitudes relatively well in the northward and eastward components (see nRMS errors and cross correlation coefficients). Here, over 20 magnetometers, distributed between 18° and 44° north magnetic latitude and around most local times, are chosen to carry out more comparisons. The choice of this latitude coverage (18°–44°) is because of three reasons. First, the equatorial electrojet current may have an influence at lower latitudes. The Sq effect, which occurs at low and middle latitudes, is subtracted from the observation data that we use for the comparison, so the effect should be minimal. Second, auroral currents will also significantly influence the perturbations during storm time if higher-latitude magnetometers are included. Third, in this study we want to show the importance of the magnetospheric current and the FACs in inducing the magnetic perturbations at the low and middle latitudes, so we want to avoid the equatorial electrojet, Sq currents, and the auroral currents as much as possible.

[16] To illustrate the comparison from all these magnetometers, we use a two-dimensional MLT-UT map. The map is created by interpolating the magnetic perturbations from all the magnetometers at different magnetic local times into 24 bins. The interpolation is done at each time (1-min) and disregards the latitude distribution of the magnetometers. The details about this interpolation technique is described by *Clauer and McPherron* [1974].

[17] Figure 4 shows MLT-UT maps of the Z component of the ground-based magnetic perturbations in solar magnetic (SM) coordinates from observations (upper left) and simulated results (bottom left). The reason for choosing the SM Z component instead of the magnetic northward component is because the magnetospheric current would produce very different northward perturbations at lower latitudes than at higher latitudes due to the geometry. A current, such as the tail current, confined to the equatorial plan and directed in an eastward or westward direction, would produce a perturbation in the northward direction at the equator and a vertical perturbation at the pole. The change between components can be removed by moving into a magnetospheric coordinate system, as in common to do when making maps such as this [*Clauer et al.*, 2006]. The two MLT-UT maps in Figure 4 (left) generally show good agreement during the storm time from 0300 UT to 0800 UT. The model not only follows the magnitude of the perturbations but also reproduces the major features. These features include (1) the storm sudden commencement (SSC) at 0315 UT, which compresses the magnetosphere suddenly and causes a significant increase of the dawn-to-dusk magnetopause current, creating a positive perturbation impulse at low-latitude and midlatitude magnetometers; (2) the negative perturbation trough in the dusk sector during the storm time when the ring current starts to build up; and (3) the positive perturbation band from 0300 UT to 0600 UT on the dawnside, where the FACs strengthen during the storm time. However, the model shows a slight magnetic local time shift from the observation; the strong negative trough observed in the observations is mainly within the magnetic local time 2100–0900 MLT through the noon, while the model predicts this trough in the region of 1900–0700 MLT. This local time difference is associated with the overrotation of the ring current in the model, as will be discussed below.

[18] To address the contributions from different current systems, the simulated MLT-UT map (Figure 4, bottom left) is split into three MLT-UT maps generated by the FACs (Figure 4, top right), the magnetospheric current (Figure 4, middle right), and the ionospheric current (Figure 4, bottom right), respectively. First, the FACs induce perturbations with a day-night asymmetry in the storm time (after 0315 UT), negative on the dayside and positive on the nightside, with the dawnside being stronger than the duskside. This asymmetry is consistent with a net downward FAC on the dawnside and a net upward FAC on the duskside. Second, the magnetospheric current induces perturbations with a slight dawn-dusk asymmetry. After the positive perturbation impulse occurs at 0315 UT over all the magnetic local times, the perturbations become negative and evolve into a dawn-dusk asymmetric pattern as the storm continues, with more negative perturbations on the duskside. This slight dawn-dusk asymmetry is associated with the ring current, which builds up on the nightside and then rotates toward the duskside in the westward direction. The strong westward convecting ring current ions drift on open paths to the dayside magnetopause, failing to reach the dawnside [e.g., *Liemohn et al.*, 1999] and generating the partial ring current. This type of development of the ring current is shown in Figure 5. At the beginning of the storm (0330 UT), a weak ring current is observed, but during the storm a partial ring current grows and significantly enhances on the duskside. Third (returning to Figure 4), the ionospheric currents induce strong perturbations in the noon-dawn sector but play an insignificant role in other magnetic local times.

[19] Besides the SM Z component, the eastward component of the ground-based perturbations is shown in Figure 6 to understand the structures of the current systems. The eastward component is shown because it is invariant of latitude and conveys significant information about the local time structure of the current systems. The three individual MLT-UT maps (Figure 6, right) shows that the main contributor to the simulated total perturbations during storm time is the FAC, which produce strong eastward perturbations in the dusk sector. The eastward perturbations extend from postnoon to postmidnight, implying a net outward FAC near 2100 MLT and a net downward FAC into the ionosphere between 0900 and 1200 MLT. These two FACs complete the ionospheric closure path for the partial ring current. However, the observation (Figure 6, top left) shows that the eastward perturbations are mainly produced in the night sector, extending from 1900 MLT to 0800 MLT through the noon, unlike the dusk section as shown in the simulation. Such discrepancy about the position of the partial ring current indicates that the model predicts a stronger westward rotation of the ring current than in reality. This overrotation also explains the local time shift shown in the Z component (see Figure 4) as mentioned above.
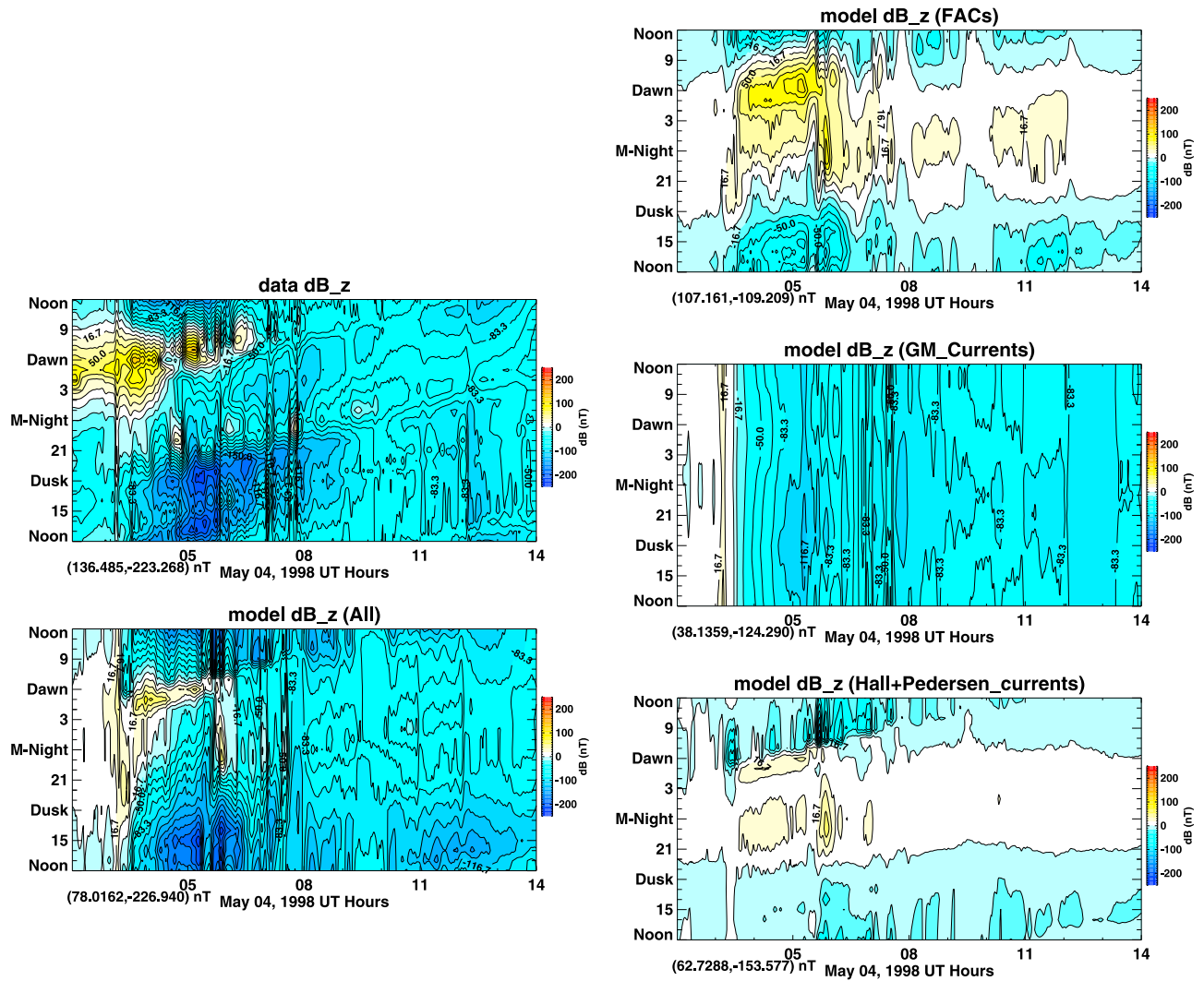
Figure 4. (left) MLT-UT maps of the Z component of the ground-based magnetic field perturbations in SM coordinates (top) from observation and (bottom) from simulation. (right) MLT-UT maps from the simulated magnetic perturbations caused by the FACs in the "gap" region only (top), by the magnetospheric currents only (middle), and by the horizontal currents in the ionosphere only (bottom). The pair of value in the parenthesis below each map shows the extremum in that map.

[20] In addition to the FACs' large contribution, the ionospheric horizontal current causes strong eastward perturbations in the noon-dawn sector. This perturbation enhancement in the noon-dawn sector can be explained by the strongly negative IMF B_y during this storm time, as the merging site is in the noon-dawn sector in such case [*Reiff and Burch*, 1985]. The magnetospheric current has little influence on the eastward perturbations.

4. Model-Data Comparison: Nine Storm Events

[21] In the previous section, only one storm event is analyzed. In this section more storm events will be compared to study the prediction capability of the model and to explore how the inclusion of different current systems in the calculation of the ground-based low-latitude and midlatitudes perturbations alters the comparison between simulated and actual observed perturbations. Table 1 lists nine storm events, in each of which, the minimum SYM-H index is shown in the parentheses to indicate the magnetospheric activity level. In each event, at least 20 magnetometers are chosen that are distributed between 18° and 44° northern magnetic latitude and over most longitudes.

[22] The three components of the magnetic perturbations are separately investigated. In each component, the simulated perturbations are calculated based on four different current sources. In other words, the current sources used in the calculation vary from (1) J_H (i.e., only the Hall current is included in the calculation, which is the common calculator for the ground-based perturbations), (2) J_a (i.e., all the current systems are included in the calculation, which what is described above), (3) J_{HF} (i.e., only the Hall current and the FACs are the included), and (4) J_{HFM} (i.e., the Hall current, the FACs, and the magnetospheric current are included). With such comparisons, the current system that matters in the improvement or degradation of the capability
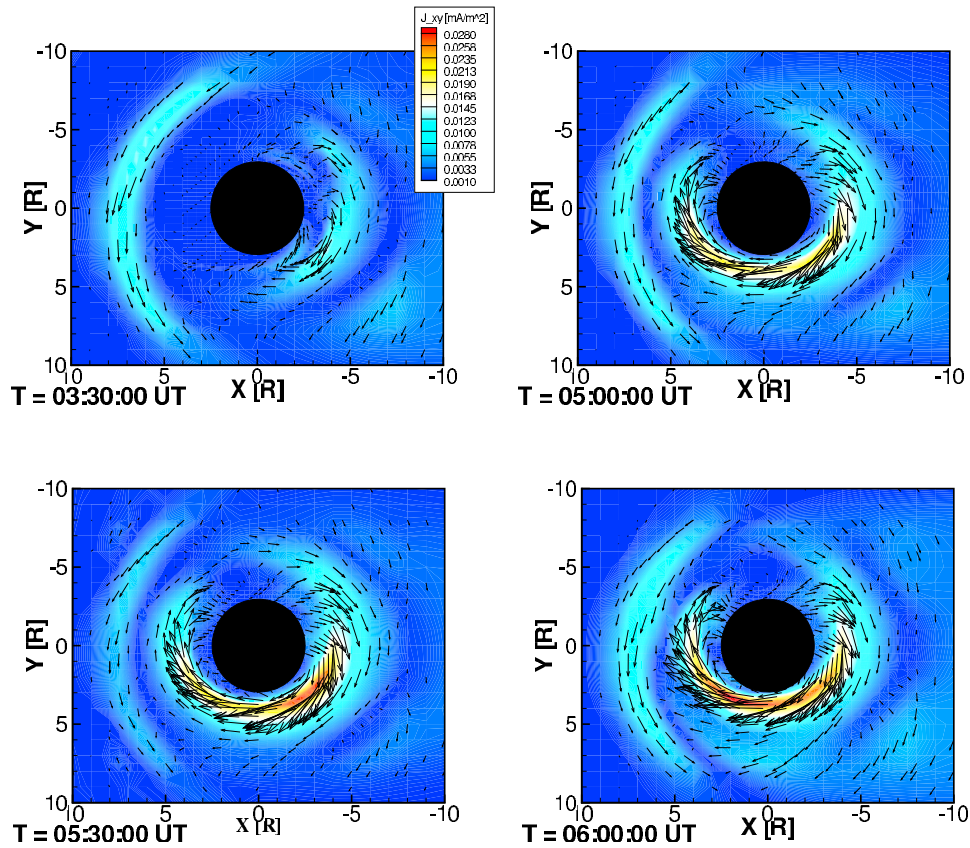
Figure 5. Current at the equatorial plane at different times in the 4 May 1998 event, with the arrows representing the vectors and color for the magnitude.

of predicting the ground-based magnetic perturbations can be determined. $\overline{nRMS}$, the averaged nRMS error over all the chosen low-latitude and midlatitude magnetometers, is used to quantify the comparison between the observation and the calculated perturbations.

[23] Table 1 shows the $\overline{nRMS}$ errors for the four different calculated perturbations in the three different components. First, in the northward component, a consistent decrease of the $\overline{nRMS}$ errors is achieved (compare the first two columns) in all the events when all the current systems are included in the calculation, indicating that the prediction of this component of the ground-based perturbations is improved. The most significant improvement lies in when J_M is taken into account (compare the second, the third, and the fourth columns). After J_M is included, the $\overline{nRMS}$ errors significantly decrease, implying that the westward ring current has a significant influence on the low-latitude and midlatitude ground-based magnetic state. Second, in the other two components, the inclusion of all current systems results in increases of the $\overline{nRMS}$ errors, which are mostly over 1, implying that the implementation of the new calculation makes the comparison even worse. To understand this degradation, individual comparisons at each magnetometer are conducted, similar to what is shown in Figures 1, 2, and 3. These comparisons reveal that the model underpredicts the magnitude in some stations and that sometimes the prediction is in the wrong direction. One explanation of the degredation is that the position of FACs that flow upward out

of or downward into the ionosphere are not solved correctly because (1) the location of the FAC with respect to the location of magnetometers determines the direction of downward perturbations observed at that magnetometer, and (2) the flow direction of the FAC determines the direction of eastward perturbations. Therefore poor prediction of the position of these FACs would cause worse $\overline{nRMS}$ errors. As a matter of fact, as mentioned above, the partial ring current in the model is over rotated toward the dayside during the storm time. Thus the ionospheric closure path (i.e., the FACs) for the partial ring current is not modeled at the correct location. This would exacerbate the degradation observed in the eastward and downward components.

[24] In addition to searching for the current system that helps to improve the prediction capability or makes the prediction worse as discussed above, an investigation is carried out to determine the time period during a storm event in which the inclusion of all the current systems actually helps to improve the comparison. Figure 7 displays three storm events in different magnetic activity levels, each with the plots of SYM-H index and the $\overline{nRMS}$ errors in three components. The $\overline{nRMS}$ error in each component is an average of the nRMS errors at all the magnetometers. The nRMS error is calculated over a 30-min window instead of over the whole simulation time period; therefore the nRMS error is a function of time instead of one value. In the northward component, the $\overline{nRMS}$ errors are mostly below 1 (as small as 0.4) during the main phase and recovery phase
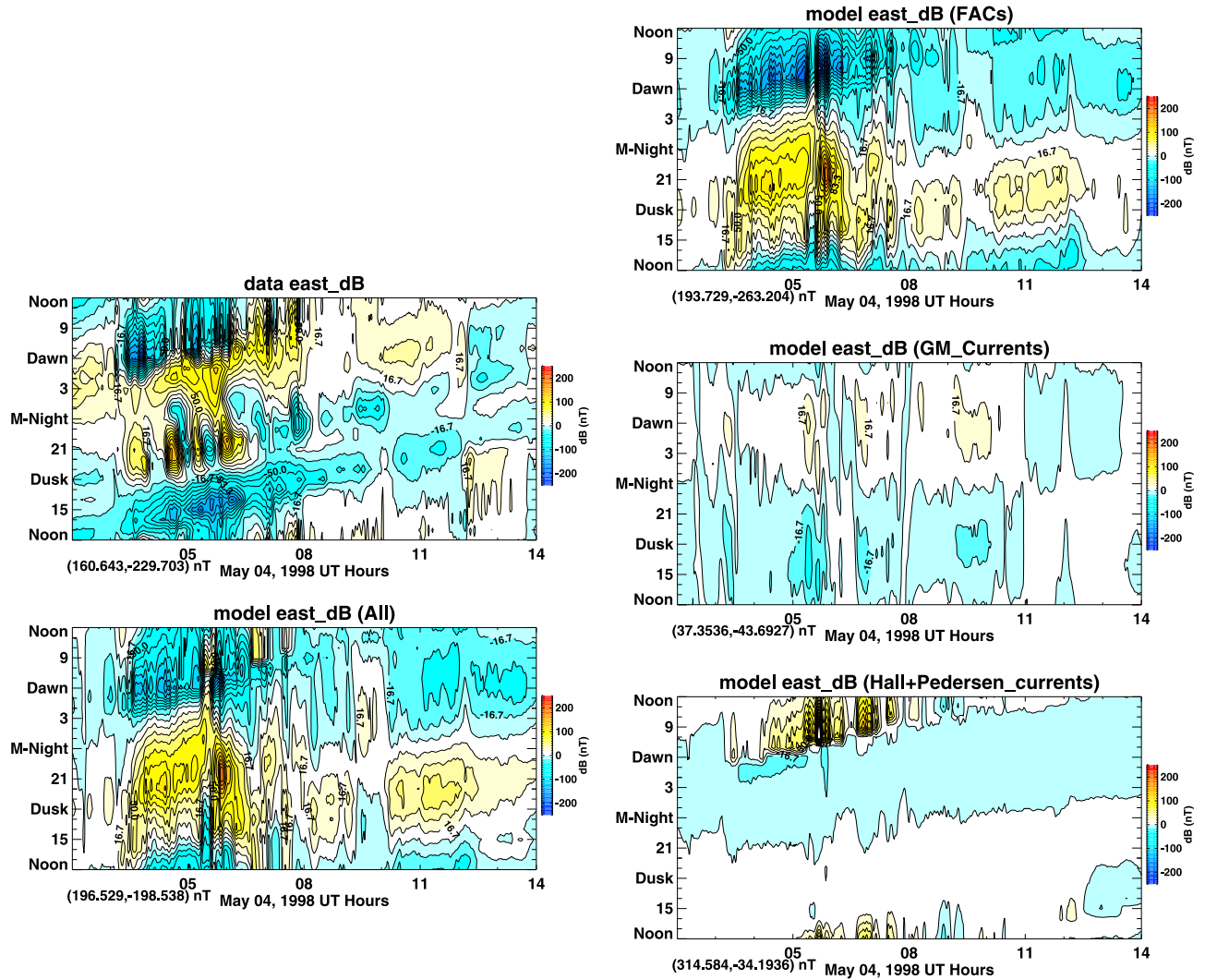
Figure 6. MLT-UT maps of the eastward component of the ground-based magnetic field perturbations in SM coordinates. The five maps are in the same format as those in Figure 4.

but are mostly above 1 during and before the sudden commencement, although the errors tend to be high during the recovery phase of the extreme storm event (20 November 2003). This main-phase improvement indicates that the

magnetospheric current, mainly the ring current, is of importance in the perturbation calculation at the low and middle latitudes, especially in magnetospherically active time. In contrast, in the other components, the $\overline{nRMS}$ errors

Table 1. Averaged Normalized RMS Errors at Middle and Low Latitudes for Nine Storm Events in Three Magnetic Field Components by Comparing the Observation Data to the Model Prediction in Which Different Current Source(s) Is Tested[a]

Component												
	B_{north}				B_{east}				B_{down}			
Sources	J_a	J_H	J_{HF}	J_{HFM}	J_a	J_H	J_{HF}	J_{HFM}	J_a	J_H	J_{HF}	J_{HFM}
19961209(−38)	0.763	0.996	0.940	0.763	1.215	1.151	1.252	1.180	2.354	1.409	1.664	2.264
19980504(−272)	0.459	0.999	0.994	0.456	1.655	1.039	1.767	1.629	2.151	0.994	1.419	2.089
20000715(−347)	0.838	1.010	1.048	0.827	2.310	1.045	2.163	2.268	1.786	1.048	1.457	1.796
20010331(−437)	0.619	0.998	1.002	0.614	2.602	1.171	2.685	2.554	2.311	1.233	1.635	2.179
20010804(−25)	0.693	0.994	0.988	0.684	1.191	1.015	1.271	1.193	1.692	1.066	1.195	1.715
20010831(−46)	0.845	0.997	0.987	0.841	1.188	1.011	1.234	1.192	1.227	1.120	1.269	1.228
20020417(−100)	0.878	1.040	1.133	0.868	1.451	1.089	1.587	1.452	1.682	1.071	1.529	1.572
20031029(−364)	0.648	0.997	1.063	0.645	1.131	1.001	1.165	1.129	2.698	1.562	1.948	2.701
20031120(−490)	0.767	0.988	1.065	0.762	0.951	0.969	0.933	0.908	1.266	1.239	1.822	1.183

[a]'J_a' represents that the perturbation is calculated from all the current systems, while 'J_H' means the Hall current is the only source, 'J_{HF}' means the Hall current and field-aligned current in the "gap" region are the source currents, and 'J_{HFM}' means the Hall current, FAC in the "gap" region and the magnetospheric current are the source currents in the calculation. Shown in the parentheses is the minimum SYM-H value for each storm event.
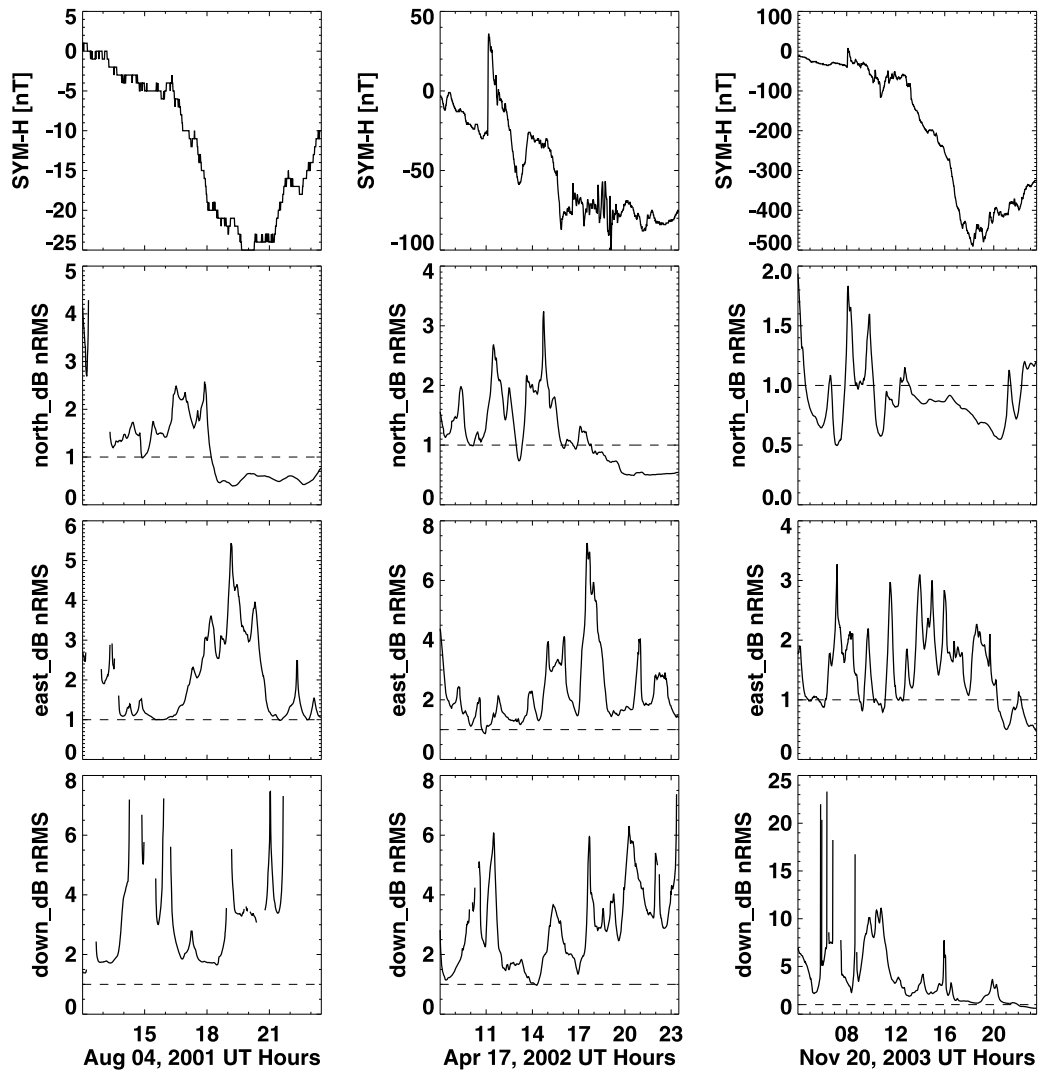
Figure 7. SYM-H index and the $\overline{nRMS}$ errors of three components of the magnetic perturbations as a function of universal time. The normalized RMS error at a certain time point is obtained by averaging over a 30-min window. Left column is a small storm on 4 August 2001 event, middle column is a moderate storm on 17 April 2002, and the right column is a extreme storm on 20 November 2003.

are almost always above 1. During the storm main phase, the errors in the eastward components can be especially high, again indicating that the partial ring current is over-rotated in a storm and that the FACs closing the path between the ring current and the ionosphere are modeled in incorrect positions. Note that in the recovery phase in the storm 31 March 2002 (last column), the $\overline{nRMS}$ errors tend to fall below 1 in both the eastward and northward components, implying that partial the ring current starts to change back to a weaker and more symmetric pattern, which is closer to that in reality.

[25] Another investigation is conducted to determine whether the model prediction possesses a local times dependence. Figure 8 shows nRMS errors as a function of local time in the three components. Initially, in each storm event, the nRMS error is calculated in a 30-min (universal time) window at each magnetometer, which results in a nRMS profile as a function of magnetic local time that the magnetometer covers. Then the nRMS error profiles from all the

magnetometers are averaged at each local time point. Finally, the profiles from all the nine storm events are averaged to obtain the nRMS error in Figure 8. From these plots, we do not find an explicit local time dependence of the nRMS errors, although in the relatively well-predicted northward component, the nRMS errors are mostly below one in the regions 0300–1300 MLT, 1500–1700 MLT, and 1900–2000 MLT. But these regions seem to be somewhat random, as inspection into each storm event reveals that different events achieve low nRMS errors in different local time regions. In the other two components, however, all the nRMS errors are above 1, only indicating that the poor predication capability in these two components has no local time dependence.

[26] To summarize, the above three investigations show that including all the current system in the calculation of the ground-based perturbations helps to improve the prediction in the northward component but does not in the eastward or downward component. It should be kept in mind that the
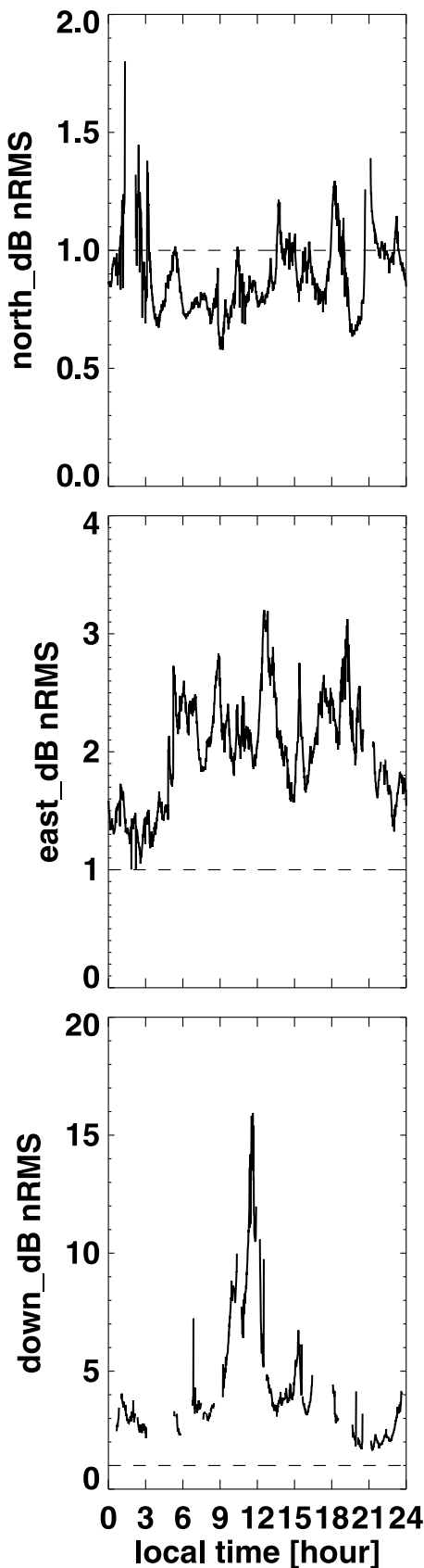
northward component is almost always dominant over the other two components. This paper therefore shows that the major current systems are being captured on a large-scale by the simulations, but the location and strength of those current systems could be incorrect.

5. Summary

[27] In MHD models, by including the ionospheric currents (Hall and Pedersen), the magnetospheric currents (ring current, tail current, magnetopause current, etc.), and the field-aligned currents from the numerical "gap" region, ground magnetic perturbations are calculated in a more precise manner than when only the Hall current is taken into account in the calculation. The analysis of different current systems in the simulation results indicates that at low and middle latitudes, the magnetospheric currents and FACs contribute mostly to the total perturbation, while at high latitudes, the Hall current dominates, since FACs and Pedersen current partly cancel each other, though not completely. The comparison of the simulation results with observations during multiple storms shows that the model does a relatively good job in reproducing the northward component of the perturbations at low and middle latitudes, implying that the model captures the gross current structure in the magnetosphere. Furthermore, we split the simulated MLT-UT maps of the perturbations at low and middle latitudes into three maps according to three different current sources (i.e., FACs, magnetospheric currents, and ionospheric currents) and found that the magnetic local time dependence of the perturbations at low and middle latitudes is a result of the combination of (1) the dusk-dawn asymmetry caused by the ring current, (2) the day-night asymmetry caused by the FACs, and (3) the localized enhancement caused by ionospheric currents in the throat region.

[28] Nine storm events were analyzed by averaging *nRMS* errors at over 20 ground-based magnetometers. The analysis shows that in the prediction of northward ground-based magnetic perturbation, the inclusion of field-aligned, magnetospheric, and ionospheric currents results in a better prediction than that under the Hall current-only assumption for low and middle latitudes. This improvement in the prediction is attributed to the inclusion of the magnetosphereic currents and has a storm-time dependence, i.e., the improvement is more profound during the storm main phase. However, the improvement does not depend on local time. The analysis also indicates that in the eastward and downward components, the model predicts worse if all the current systems are considered. This degradation is associated with the location of the partial ring current and the FACs. The partial ring current in the model is systematically rotated in a westward direction more than in reality, and therefore the ionospheric closure path (i.e., by FACs) is

Figure 8. The nRMS errors as a function of magnetic local time in three components of the magnetic perturbations. The error is initially calculated at each magnetometer over a 30-min window, then is averaged over the magnetometers at the same local time point, and finally is averaged over all the nine storm events.

shifted by some local hours toward dusk, inducing the eastward and downward perturbations in an incorrect direction. This stronger rotation of the partial ring current implies that the flow channels in the magnetospheric model need to be directed more toward dawn, allowing the ring current to develop more toward midnight. One possible reason for this strong rotation of the ring current is the ionospheric conductance specification, which can strongly control the dynamics of the ring current [*Liemohn et al.*, 2005; *Ebihara and Ejiri*, 2003].

[29] We should keep in mind that the northward component of the ground-based perturbations is always dominant and more important, and therefore the method shown in this study of including those current systems in the calculation allows a more precise and reasonable prediction. Using this technique, we can both validate the large-scale current systems in the magnetosphere-ionosphere system and study their dynamic behavior. In addition, the model provides a tool to study the latitude and magnetic local time-dependent magnetic perturbations.

References

Chen, C.-K., R. A. Wolf, J. L. Karty, and M. Harel (1982), Theoretical magnetograms based on quantitative simulation of a magnetospheric substorm, *J. Geophys. Res.*, *87*, 6137–6152.

Clauer, C. R., and R. L. McPherron (1974), Mapping the local time - universal time development of magnetospheric substorms using mid-latitude magnetic observations., *J. Geophys. Res.*, *79*, 2811–2820.

Clauer, C. R., X. Cai, D. Welling, A. DeJong, and M. G. Henderson (2006), Characterizing the 18 April 2002 storm-time sawtooth events using ground magnetic data, *J. Geophys. Res.*, *111*, A04590, doi:10.1029/2005JA011099.

Ebihara, Y., and M. Ejiri (2003), Numerical simulation of the ring current: Review, *Space Sci. Rev.*, *105*, 377–452, doi:10.1023/A:1023905607888.

Fukushima, N. (1976), Generalized theorem for no ground magnetic effect of vertical currents connected with Pedersen currents in the uniform-conductivity ionosphere, *Rep. Ionos. Space Res. Jpn.*, *30*, 35–40.

Kobea, A. T., C. Amory-Mazaudier, J. M. Do, H. Lühr, E. Houngninou, J. Vassal, E. Blanc, and J. J. Curto (1998), Equatorial electrojet as part of the global circuit: A case study from the IEEY, *Ann. Geophys.*, *16*, 698–710, doi:10.1007/s005850050639.

Liemohn, M. W., J. U. Kozyra, V. K. Jordanova, G. V. Khazanov, M. F. Thomsen, and T. E. Cayton (1999), Analysis of early phase ring current recovery mechanisms during geomagnetic storms, *Geophys. Res. Lett.*, *26*, 2845–2848.

Liemohn, M. W., A. J. Ridley, P. C. Brandt, D. L. Gallagher, J. U. Kozyra, D. M. Ober, D. G. Mitchell, E. C. Roelof, and R. DeMajistre (2005), Parametric analysis of nightside conductance effects on inner magnetospheric dynamics for the 17 April 2002 storm, *J. Geophys. Res.*, *110*, A12S22, doi:10.1029/2005JA011109.

Powell, K. G., P. L. Roe, T. J. Linde, T. I. Gombosi, and D. L. D. Zeeuw (1999), A solution-adaptive upwind scheme for ideal magnetohydrodynamics, *J. Comput. Phys.*, *154*, 284–309.

Pulkkinen, A., M. Hesse, M. Kuznetsova, and L. Rastätter (2007a), First-principles modeling of geomagnetically induced electromagnetic fields and currents from upstream solar wind to the surface of the Earth, *Ann. Geophys.*, *25*, 881–893.

Pulkkinen, A., R. Pirjola, and A. Viljanen (2007b), Determination of ground conductivity and system parameters for optimal modeling of geomagnetically induced current flow in technological systems, *Earth Planets Space*, *59*, 999–1006.

Raeder, J., Y. L. Wang, T. J. Fuller-Rowell, and H. J. Singer (2001), Global simulation of magnetospheric space weather effects of the Bastille Day storm, *Sol. Phys.*, *204*, 323–337.

Reiff, P.-H., and J.-L. Burch (1985), IMF B(y)-dependent plasma flow and Birkeland currents in the dayside magnetosphere. II - A global model for southward and northward IMF, *J. Geophys. Res.*, *90*, 1595–1609.

Ridley, A. J., D. L. De Zeeuw, T. I. Gombosi, and K. G. Powell (2001), Using steady-state MHD results to predict the global state of the magnetosphere-ionosphere system, *J. Geophys. Res.*, *106*, 30,067–30,076.

Ridley, A. J., K. C. Hansen, G. Tóth, D. L. D. Zeeuw, T. I. Gombosi, and K. G. Powell (2002), University of Michigan MHD results of the Geospace Global Circulation Model Metrics Challenge, *J. Geophys. Res.*, *107*(A10), 1290, doi:10.1029/2001JA000253.

Ridley, A. J., T. I. Gombosi, and D. L. D. Zeeuw (2004), Ionospheric control of the magnetospheric configuration: Conductance, *Ann. Geophys.*, *22*, 567–584.

Shao, X., P. N. Guzdar, G. M. Milikh, K. Papadopoulos, C. C. Goodrich, A. Sharma, M. J. Wiltberger, and J. G. Lyon (2002), Comparing ground magnetic field perturbations from global MHD simulations with magnetometer data for the 10 January 1997 magnetic storm event, *J. Geophys. Res.*, *107*(A8), 1177, doi:10.1029/2000JA000445.

Wiltberger, M., J. G. Lyon, and C. C. Goodrich (2003), Results from the Lyon-Fedder-Mobarry global magnetospheric model for the electrojet challenge, *J. Atmos. Sol. Terr. Phys.*, *65*, 1213–1222.

Wolf, R. A., M. Harel, R. W. Spiro, G. Voigt, P. H. Reiff, and C. K. Chen (1982), Computer simulation of inner magnetospheric dynamics for the magnetic storm of July 29, 1977, *J. Geophys. Res.*, *87*, 5949–5962.

Yu, Y., and A. J. Ridley (2008), Validation of the space weather modeling framework using ground-based magnetometers, *Space Weather*, *6*, S05002, doi:10.1029/2007SW000345.

A. J. Ridley, G. Tóth, and Y. Yu, Center for Space Environment Modeling, University of Michigan, Ann Arbor, MI 48109, USA. (yiqunyu@umich.edu)

D. T. Welling, Los Alamos National Laboratory, Los Alamos, NM 87545, USA.